Journal of Geodynamics 94–95 (2016) 1–12

Contents lists available at ScienceDirect

Journal of Geodynamics

journal homepage: http://www.elsevier.com/locate/jog

Slip rates and seismic potential on the East Anatolian Fault System using an improved GPS velocity field

B. Aktug[a,*], H. Ozener[b], A. Dogru[b], A. Sabuncu[b], B. Turgut[b], K. Halicioglu[b], O. Yilmaz[b], E. Havazli[b]

[a] Ankara University, Department of Geophysical Engineering, 06830 Gölbaşı, Ankara, Turkey
[b] Bogazici University Kandilli Observatory and Earthquake Research Institute Geodesy Department, 34684 Cengelkoy, Istanbul, Turkey

ARTICLE INFO

Article history:
Received 8 June 2015
Received in revised form 18 January 2016
Accepted 25 January 2016
Available online 27 January 2016

Keywords:
East Anatolian Fault
Slip rates
Locking depth
Seismic potential
Dead Sea Fault

ABSTRACT

The East Anatolian Fault System (EAFS) is the second major fault system in Turkey, following the North Anatolian Fault System (NAFS). Unlike the NAFS, which produced 11 large earthquakes in the last ~75 years, the EAFS has been relatively quiet during the same period of time. While historical records show that the EAFS has the potential to produce large earthquakes, the fault slip rates on the EAFS were not studied in detail, and were not quantified sufficiently. This is possibly due to the relatively low seismicity and slow slip-rates of the EAFS with respect to the NAFS. However, the determination of the slip rates of the EAFS is equally important in order to understand the kinematics of the Anatolian plate.

In this study, we collected and analyzed new survey-type GPS data, and homogeneously combined published velocities from other studies, to form the most complete GPS data set covering the EAFS. In particular, continuous GPS observations were utilized for the first time to study the northern part of the EAFS. The results of the analysis give well-constrained slip rates of the northwestern segments of the EAFS, which is further connected to the Dead Sea Fault System (DSFS) in the south.

The results show that while the slip rate of the EAFS is nearly constant (~10 mm/yr) to the north of Türkoğlu, it then decreases to 4.5 mm/yr in the south. The slip rate on the northern part of the Dead Sea Fault System (DSFS) was also found to be 4.2 ± 1.3 mm/yr, consistent with earlier studies. The contraction rates along the EAFS are below 5 mm/yr, except for the northernmost part near Karliova, where it reaches a maximum value of 6.3 ± 1.0 mm/yr. The results also show that two well-known seismic gaps across the EAFS, Palu-Sincik and Çelikhan-Türkoğlu segments, have slip deficits of 1.5 m and 5.2 m and have the potential to produce earthquakes with magnitudes of M_w7.4 and M_w7.7, respectively.

1. Introduction

The East Anatolian Fault System delineates the boundary between the Anatolian and Arabian plates, and is associated with thrusting and left-lateral faulting. It is often considered a continuation of the Dead Sea Fault System to the north where the subduction of the African plate beneath Anatolia and the differential motion of the Arabian plate with respect to the African plate are the main driving mechanisms (McKenzie, 1972; Şengör and Kidd, 1979; Dewey et al., 1986). Together with the North Anatolian Fault System, the EAFS is one of the most active transform fault systems in Turkey. While the tectonic escape of the Anatolian plate is usually attributed to the squeezing of the Anatolian wedge along the EAFS and slab pull in the Hellenic Arc, recent studies show that the normal components of slip rates along the EAFS are much less than the required effect and that slab pull should be the dominant factor (Reilinger et al., 2006; Aktuğ et al., 2013). Although the EAFS was relatively quiet during the last century, historical seismicity shows that the EAFS is capable of producing devastating earthquakes (Ambraseys, 1989).

Recent stress transfer studies also verify the large strain accumulation across the EAFS (Nalbant et al., 2002). Two seismic gaps are identified across the EAFS: Palu-Sincik and Çelikhan-Türkoğlu segments (Fig. 1). The Palu-Sincik segment is a 135-km long segment between Palu and Sincik, consisting of the Palu-Sivrice and Sivrice-Sincik segments, which are 50 km and 85 km long, respectively. While exact locations are still under dispute, two large earthquakes, 1874 (M7.1) and 1875 (M6.7), have occurred within this segment. They are considered to have occurred in the southern part of Sivrice (Nalbant et al., 2002; Herece, 2008), while Ambraseys

* Corresponding author.
E-mail address: aktug@ankara.edu.tr (B. Aktug).

http://dx.doi.org/10.1016/j.jog.2016.01.001
0264-3707/

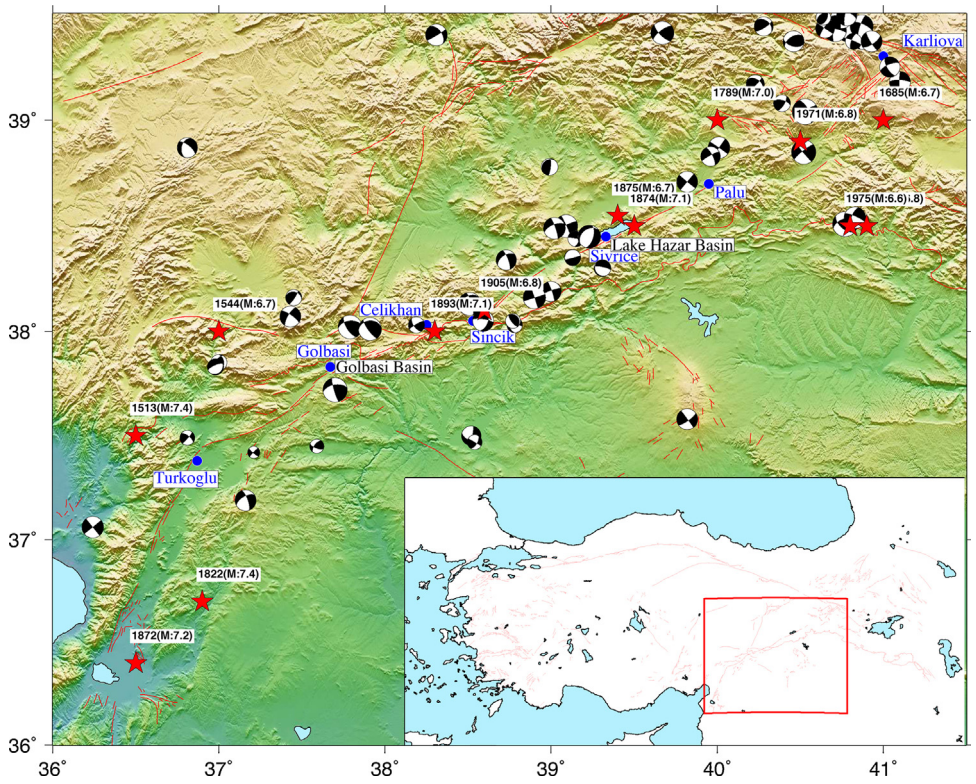

Fig. 1. The seismotectonic framework of the Eastern Anatolia and the surrounding regions. The source parameters of the earthquakes are from the catalogue given by Kalafat et al. (2009) which spans the period between 1938 and 2008 and includes events $M > 4.0$. The asterisks show the historical earthquakes and are from Ambraseys (1989). The fault traces were adapted from Şaroğlu et al. (1992b).

and Jackson (1998) and Çetin et al. (2003) suggested a location to the north of Sivrice. The Çelikhan-Türkoğlu segment is 140 km long, consisting of the Çelikhan-Gölbaşı and Gölbaşı-Türkoğlu segments, which are 50 km and 90 km long, respectively. The most recent earthquake on the Çelikhan-Gölbaşı segment occurred in 1513 (M7.4). Determination of the slip rates along these segments at highest precision is critical to evaluate the seismic potential reliably.

The complex geological setting and relatively low seismicity do not allow precise determination of the slip history or the recurrence intervals across the EAFS. The estimates of slip rate, based on the cumulative seismic moment sums, range from 29 mm/yr to 70 mm/yr (Jackson and McKenzie, 1984, 1988; Taymaz et al., 1991). The slip rates, based on the geological offset measurements of two pull-apart basins, Gölbaşı and Lake Hazar Basins, are also highly variable. The slip rates, based on the measurement of total offsets, range between 4 mm/yr and 13 mm/yr (Hempton, 1985; Arpat-Şaroğlu, 1972; Dewey et al., 1986; Allen et al., 2004; Westaway, 1994; Aksoy et al., 2007).

Early estimates of the EAFS slip rates were reported as 9–11 mm/yr, and were based on the relative rigid block rotations of the Anatolian and Arabian plates (Oral et al., 1995; Reilinger et al., 1997; McClusky et al., 2000). Such a methodology assumes a uniform slip rate over the whole fault boundary. Later studies also employed rigid block rotations, but the elastic strain accumulation near block boundaries were also taken into consideration (Reilinger et al., 2006; Aktuğ et al., 2013). Reilinger et al. (2006) reported left-lateral slip rates of 9.9 ± 0.2 mm/yr and 10.0 ± 0.3 mm/yr in the northern part, and contraction rates of 5.1 ± 0.3 mm/yr and 2.9 ± 0.3 mm/yr, based on a relatively coarse block boundary discretization. However, all these studies still lack sufficient density and coverage to identify and to quantify the slip rates of individual segments of the EAFS. There are also two recent InSAR studies which overcome the spatial resolution problem of previous GPS studies. Cavalié and Jónsson (2014) reported a slip rate and a locking depth of 13 mm/yr and 4.5 km, respectively, for the northern segment between 39° E and 41° E. In a more recent study, Walters et al. (2014) found an average slip rate and locking depth of 11 ± 3 mm/yr and 15 ± 5 km, respectively, for the segments to the north of 36° N. However, slip rates and locking depths as little as 8 mm/yr and 8 km are also observed in the northernmost segments (Walters et al., 2014).

In this study, we present the most complete GPS data set studies to date, which were obtained from analysis of new GPS data and a rigorous combination of available published data sets. We investigated the possible variations of the slip rate and the locking depth through a robust analysis to quantify the strain accumulation and possible release in the middle and eastern part of the EAFS. The homogeneously combined data allow the precise determination of the slip rates of individual segments of the EAFS, which has not been possible in the earlier studies.

2. Tectonic framework

The kinematics of Anatolia and its surrounding regions have been of interest to many researchers due to the diversity of its tectonic setting. In this region we find rigid-body rotation, collision and subduction of a continental plate, major strike-slip and thrust faulting, compression and extension (Barka and Kadinsky-Cade, 1988; Şengör et al., 1985). The region is bounded by the North Anatolian Fault Zone (NAFZ) to the north, and the East Anatolian Fault Zone (EAFZ) to the east, and the Hellenic and the Cyprian Arcs in the south, where the Arabian, African and Eurasian plates converge.

The East Anatolian Fault System (EAFS) delineates the boundary between the Arabian and Anatolian plates. Often considered a conjugate structure to the North Anatolian Fault System (NAFS),

the EAFS is a 600 km long SW–NE trending fault zone between Karliova in the north, and Kahramanmaraş in the south (McKenzie, 1970; Arpat and Saraǧlu, 1972; Westaway, 1994). The EAFS is a predominantly strike-slip fault system with well-observed pull-apart basins, including the Gölbaşı and Hazar Lake basins (Bozkurt, 2001).

The uplift of the East Anatolian plateau is often considered to have started about 13 Ma ago, just after the collision of Arabian and Anatolian plates (Şengör and Kidd, 1979; Dewey et al., 1986). Robertson (2000) suggested that the collision started as early as the early Miocene (16–23 Ma). The estimates for the onset of the collision range from 65 Ma (Berberian and King, 1981) to 40 Ma (Hempton, 1987) and to 16–23 Ma (Robertson, 2000) and to as little as 5 Ma (Philip et al., 1989). A re-organization of the collision about 5 Ma ago was also reported by Allen et al. (2004) based on geological evidence for the change in the rates of strain in folds and exhumation of mountain belts. It was suggested by Allen et al. (2004) that 16–23 Ma could be the earliest range for the onset of the collision. The crustal thickening due to the collision is considered to reach ~45 km based on seismic data (Sandvol et al., 2003; Zor et al., 2003). Another striking finding in these studies is the thinning of the crust from ~44 km in the north to 36 km in the south. The average crustal thickness along the EAFS was estimated as 36 km by Gök et al. (2007).

Several onset times for the EAFS were proposed, ranging from Late Pliocene (Şaroğlu et al., 1987; Westaway and Arger, 2001) to the latest Pliocene-Pleistocene (Herece, 2008). But the onset of the EAFS slip is still under debate and ranges between 1.8 and 12 Ma (Arpat and Saraǧlu, 1972; Hempton, 1987; Lybéris et al., 1992; Yürür and Chorowicz, 1998). Şengör et al. (1985) asserted that the EAFS initiated 5 Ma ago, based on the Pliocene-aged sediments in the fault related basins. This value was further refined by Şaroğlu et al. (1992a), who claimed that initial movement on the East Anatolian Fault was late Pliocene (3 Ma) or younger. Early comparison of the geological slip rates with those of GPS also suggests that it started in the Pliocene era (4–5 Ma) (Reilinger et al., 1997). The estimates of age for individual fault segments range from 3 to 5 Ma to late Eocene (Westaway and Arger, 2001; Jaffey and Robertson, 2001; Allen et al., 2004).

The segmentation of the EAFS is also under debate. Barka and Kadinsky-Cade (1988) suggested a 14-segment structure for the EAFS, while Şaroğlu et al. (1992a) and Hempton et al. (1981) reported six and five segments respectively. Recent geometrical segment classifications of the EAFS include the 11-segment geometry of Herece (2008) and a 7-segment geometry of Duman and Emre (2013). The 7-segment geometry of Duman and Emre (2013) seem to be the most complete and refined model up to date since it already compares and discusses the previous findings.

The estimates for total geological offset across the EAFS vary; 15–22 km (Hempton, 1985), 22–27 km (Arpat and Saraǧlu, 1972), 22 km (Dewey et al., 1986), and 27–33 km (Allen et al., 2004). The 33-km long Gölbaşı pull-apart basin can be considered another measure for the total offset, as given in Westaway and Arger (1996). Geological data suggest a slip rate of 6–10 mm/yr, based on 35–40 km offset (Westaway and Arger, 1996). Westaway (1994) suggested a slip rate of 13 ± 1 mm/yr for the EAFS. Another basin frequently used for estimation of the total offset is the Lake Hazar Basin. The total geological offset across the Lake Hazar Basin is estimated to vary between 9 km and 27 km (Arpat and Saraǧlu, 1972; Hempton, 1985; Herece and Akay, 1992). Aksoy et al. (2007) reported a left-lateral slip rate of 4 mm/yr, based on a total offset of 6.5–9 km across Plio–Quaternary (~2.6 Ma) markers.

The EAFS was seismically relatively quiescent during the last century compared with the NAFS. The most notable earthquakes are the 1971 Bingöl (M:6.8) and the 1986 Sürgü (M:6.0) events. However, large historical pre-instrumental earthquakes were reported along the EAFS by Ambraseys (1989) and Nalbant et al. (2002). Among those are the 1874 (M7.1) and the 1875 (M6.7) earthquakes near Lake Hazar, and the 1513 (M7.4) earthquake near Gölbaşı. Historical earthquakes from the literature and large earthquakes of the instrumental period with available focal mechanism solutions are shown in Fig. 1.

3. GPS observations and analysis

Raw GPS observations, which complement the published velocity fields, were obtained from the national mapping institution of Turkey (General Command of Mapping) for the years 1998, 1999, 2002, 2003, 2006, 2007 and 2010. All the observations were collected at sessions of at least 8 h using dual frequency GPS receivers. GPS data reduction and estimation of the velocity field was carried out in a three-step approach described by Dong et al. (1998). In the first step, the individual GPS campaign observations were processed daily and were combined as yearly solutions by using GAMIT/GLOBK software (King et al., 2009). The IGS final orbit products and IERS orientation products were incorporated into the analyses, together with a sufficient number of IGS fiducial site observations. The normal equations matrix with loose constraints was produced for each yearly campaign solution. In the second step, taking loosely-constrained campaign solutions as quasi-observations, a combined normal equation matrix was obtained in a Kalman Filter scheme method by using GLOBK software (Herring, 1997).

In the last step, the reference frames of both coordinate and velocity estimates were defined by estimating a 12-parameter transformation (three translations, three rotations and their associated rates) to ITRF2008 coordinates of 17 selected IGS sites (NSSP, ZECK, NICO, SOFI, JOZE, KIRU, LAMA, TROM, MATE, GRAZ, POTS, WTZR, ONSA, CAGL, ZIMM, GRAS, BRUS). The selection of sites for reference frame definition was made based on the factors given in Aktuğ et al. (2009). The post-fit rms (root mean square) of 17 stations was found to be 1 mm and 0.17 mm/yr for the coordinates and the velocities, respectively.

3.1. Combination of velocity fields

The velocity fields published in previous studies were also incorporated into the analysis to provide a denser velocity field and to determine the slip rates more reliably. Aktuğ et al. (2013) provided a velocity field covering the westernmost part of the EAFS. While the velocity field given in Reilinger et al. (2006) is very sparse in the region, especially to constrain the motion of the Arabian block, it still has many sites in the region. Alchalbi et al. (2009) provided a dense velocity field covering the southern part of the EAFS. The velocity vectors of the Turkish RTK Network (GCM, 2013) were also incorporated into the combined velocity field with block diagonal covariance matrices. More recently, Mahmoud et al. (2013) published a dense velocity field focusing on the Dead Sea Fault System. However, it was not used here because the average precision of the velocity field is much less than other individual solutions, and the sites located near the EAFS are common with other velocity fields used in this study. The velocity fields obtained from all studies are shown in Fig. 2.

It is necessary to remove any possible reference frame effect to effectively combine the published velocity fields (Aktuğ et al., 2009). In this respect, the computed velocity field and the published velocity fields gathered from the literature were transformed into the reference frame given in Reilinger et al. (2006), due to the fact that the velocity field given there has the highest number of common sites with other solutions.

Both translations and rotations could exist between two reference frames. However, any translation can be represented as a

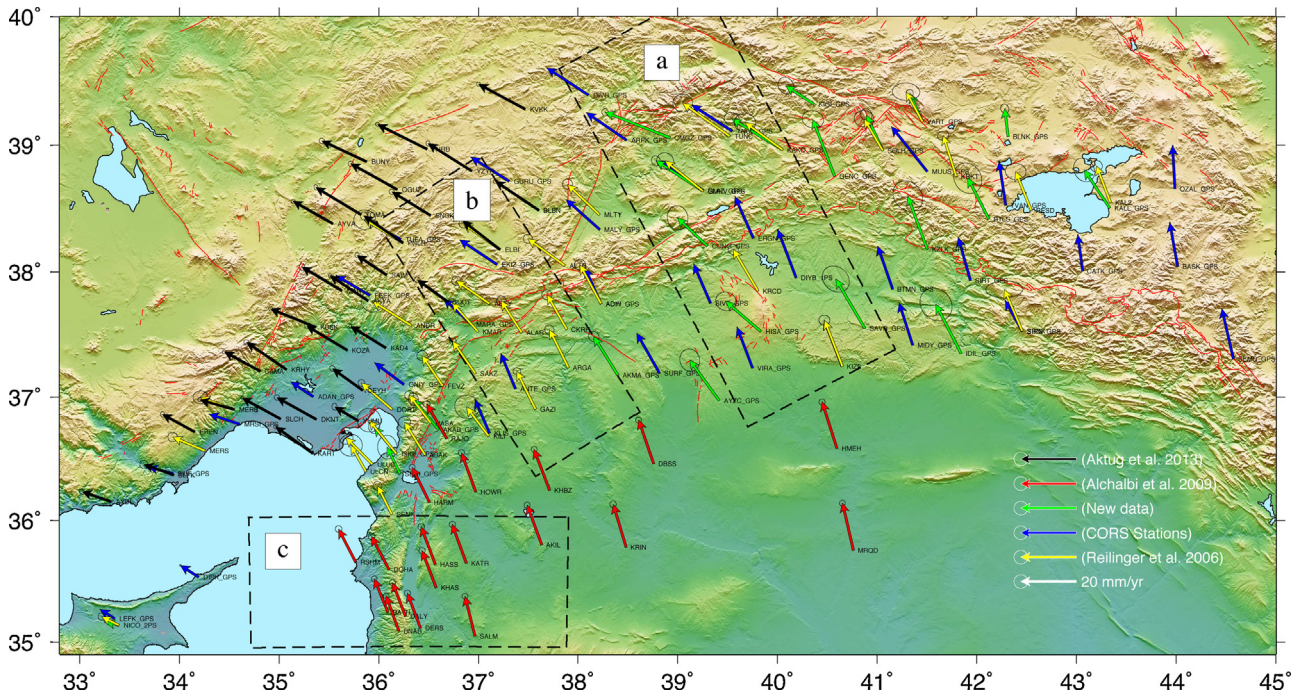

Fig. 2. The GPS observations employed in this study. The velocity error ellipses are at 95% confidence level. The dashed rectangles show the profiles for investigating the trade-off between the slip rate and the locking depth.

rotation over a sphere in Euler theorem. Since any translations could be absorbed in Euler rotations, estimating a simple Euler rotation matrix between a velocity field and the reference velocity is sufficient. The transformation model used for the combination is:

$$v_2 = v_1 + R(\Omega \times r) \tag{1}$$

where v_1 and v_2 are the velocity vectors in both local frames, R is the rotation matrix to transform from geocentric Cartesian to local coordinate systems and Ω is the Euler rotation vector, the "$\times$" stands for vector product and r is the position vector at each station. Using (1), the individual velocity fields were transformed into the reference frame given in Reilinger et al. (2006) by minimizing the misfit between the velocities of common sites via least-squares. The consistency of the combined solutions is given in Table 1 and the transformed velocities are given in Table 2.

3.2. Slip rate and locking depth variation

Due to the trade-off of the slip rate with the locking depth, the simultaneous estimation of both quantities could be misleading, depending on the geometric coverage of velocities. For an infinitely long vertical strike-slip fault, the classical relationship (Savage and Burford, 1973) between the fault-parallel velocities and distance to the fault is given by

$$v = V_{off} + \frac{V}{\pi} \tan^{-1}\left(\frac{x + \Delta x}{D}\right) \tag{2}$$

where x is the perpendicular distance to the fault trace, V is the slip rate, D is the locking depth and v is observed fault parallel velocity, Δx is the fault offset and V_{off} is the offset necessary to define velocities in the same model velocity reference frame (Segall, 2010). Estimating V_{off} term ensures that the velocities on the fault ($x = 0$) are zero and the velocities on either side of the fault have opposite signs. The term Δx was added to Eq. (2) to account for any possible error due to the simplification of fault delineation while projecting the fault normal distances. The locking depths and slip rates were estimated simultaneously for profiles labeled (a) through (c) in Fig. 2 through a non-linear regression algorithm (Seber and Wild, 2003). The confidence bounds were also estimated using a bootstrapping method. The results are shown in Table 3. The estimated velocity and fault offsets range between 3–13 mm/yr and 2–5 km. Using the estimated velocity and fault offsets, we estimated the slip rate for a constant locking depth varying between 0.1 km and 60 km to investigate the trade-off between the locking depth and the slip rate. The calculated slip rates for a range of locking depths, and the associated misfits for the two profiles are shown in Fig. 3.

Since the most of the western part of profile b lies at sea, only a limited number of observations are available on the west side of

Table 1
The rotation rates of the individual solutions computed from the common sites to the reference velocity field (Reilinger et al., 2006). The individual data sets were transformed into the reference velocity frame using the computed rotation rates. The number of sites column (#) shows the total number of common sites between each solution and the reference velocity field (Reilinger et al., 2006).

λ (°)	ϕ (°)	Ω (10^{-9}°/Myr)	# of sites	rms (mm/yr)	Source
−50.0506	5.4849	2.0	16	0.63	New solution
−56.8488	−2.6429	3.6	14	0.49	Aktuğ et al. (2013)
−35.1577	−10.3350	4.5	5	0.43	Alchalbi et al. (2009)
53.5288	79.3748	38.94	14	0.47	GCM (2013)
–	–	–	–	–	Reilinger et al. (2006)[a]

[a] Reference velocity field.

Table 2
The transformed velocities and their sources used in the analysis.

Site	Lon. (°)	Lat. (°)	v_e (mm/yr)	v_n (mm/yr)	σ_{Ve} (mm/yr)	σ_{Vn} (mm/yr)	ρ_{VeVn}	Source
AKYA	35.896	37.771	−13.7	9.1	0.2	0.3	−0.037	Aktuğ et al. (2013)
AYDI	33.315	36.152	−10.5	3.6	0.4	0.4	−0.069	Aktuğ et al. (2013)
AYVA	35.542	38.382	−14.3	8.1	0.3	0.3	−0.054	Aktuğ et al. (2013)
BLBN	37.607	38.488	−15.7	10.5	0.3	0.3	−0.041	Aktuğ et al. (2013)
BUNY	35.881	38.870	−16.1	7.5	0.4	0.4	−0.116	Aktuğ et al. (2013)
CAMA	34.811	37.207	−12.9	6.9	0.3	0.3	−0.020	Aktuğ et al. (2013)
CEYH	35.839	37.055	−10.9	7.9	0.4	0.4	−0.094	Aktuğ et al. (2013)
DKNT	35.375	36.820	−14.2	7.9	0.4	0.4	−0.071	Aktuğ et al. (2013)
ELBI	37.220	38.179	−13.4	10.4	0.2	0.3	−0.098	Aktuğ et al. (2013)
EREN	34.155	36.718	−11.6	6.4	0.3	0.4	−0.049	Aktuğ et al. (2013)
GAZI	32.283	36.283	−8.5	0.3	0.3	0.3	−0.116	Aktuğ et al. (2013)
KAD4	36.073	37.394	−12.8	7.9	0.2	0.3	0.000	Aktuğ et al. (2013)
KART	35.340	36.543	−13.4	9.7	0.3	0.3	−0.100	Aktuğ et al. (2013)
KBSK	35.369	37.560	−16.2	6.6	0.3	0.3	−0.067	Aktuğ et al. (2013)
KOZA	35.685	37.376	−14.6	8.8	0.3	0.4	−0.114	Aktuğ et al. (2013)
KRHY	35.076	37.221	−14.4	9.8	0.4	0.4	−0.083	Aktuğ et al. (2013)
KVKK	37.470	39.283	−16.8	9.0	0.3	0.3	−0.008	Aktuğ et al. (2013)
MANS	35.632	37.851	−14.4	8.6	0.4	0.5	−0.069	Aktuğ et al. (2013)
MERS	34.552	36.900	−12.3	3.5	0.3	0.3	−0.084	Aktuğ et al. (2013)
OGUZ	36.188	38.651	−16.7	9.3	0.4	0.4	−0.119	Aktuğ et al. (2013)
PNLR	36.245	38.231	−14.1	9.7	0.5	0.6	−0.071	Aktuğ et al. (2013)
PNRB	36.484	38.971	−17.8	8.9	0.3	0.3	−0.168	Aktuğ et al. (2013)
SAIM	36.082	37.977	−10.7	7.1	0.3	0.4	−0.129	Aktuğ et al. (2013)
SLCH	35.018	36.824	−13.8	7.6	0.2	0.3	−0.060	Aktuğ et al. (2013)
SLFK	33.944	36.370	−10.8	3.8	0.6	0.6	−0.048	Aktuğ et al. (2013)
SNCK	36.521	38.447	−13.9	8.6	0.4	0.4	−0.083	Aktuğ et al. (2013)
SUCT	36.697	37.761	−11.1	8.0	0.4	0.4	−0.053	Aktuğ et al. (2013)
TOMA	35.825	38.455	−16.3	9.8	0.3	0.4	−0.114	Aktuğ et al. (2013)
YUMU	35.795	36.808	−8.5	5.1	0.4	0.5	−0.091	Aktuğ et al. (2013)
YZYR	36.934	38.799	−15.7	9.9	0.3	0.4	−0.079	Aktuğ et al. (2013)
AKIL	37.634	35.800	−5.2	14.3	0.4	0.5	−0.006	Alchalbi et al. (2009)
BATH	36.091	35.247	−4.9	12.1	0.4	0.4	0.006	Alchalbi et al. (2009)
BNAB	36.204	35.090	−4.6	12.8	0.4	0.4	0.003	Alchalbi et al. (2009)
DALY	36.270	35.215	−4.7	12.1	0.5	0.5	−0.004	Alchalbi et al. (2009)
DBSS	38.757	36.461	−5.4	15.7	0.4	0.4	−0.001	Alchalbi et al. (2009)
DERS	36.419	35.118	−4.7	12.5	0.5	0.5	−0.006	Alchalbi et al. (2009)
DOHA	36.104	35.598	−6.3	12.0	0.5	0.5	0.012	Alchalbi et al. (2009)
HARM	36.508	36.146	−6.2	12.6	0.5	0.4	0.004	Alchalbi et al. (2009)
HASS	36.570	35.638	−5.1	13.6	0.5	0.5	−0.006	Alchalbi et al. (2009)
HMEH	40.596	36.584	−5.3	16.8	0.5	0.5	−0.003	Alchalbi et al. (2009)
HOWR	36.974	36.233	−5.2	14.1	0.5	0.5	0.001	Alchalbi et al. (2009)
KATR	36.881	35.649	−5.1	14.0	0.5	0.4	−0.008	Alchalbi et al. (2009)
KHAS	36.578	35.449	−5.1	13.4	0.5	0.5	−0.004	Alchalbi et al. (2009)
KHBZ	37.716	36.246	−5.6	14.7	0.4	0.4	−0.011	Alchalbi et al. (2009)
KRIN	38.481	35.782	−4.6	15.4	0.5	0.5	−0.018	Alchalbi et al. (2009)
MRQD	40.761	35.754	−3.9	17.0	0.4	0.4	−0.006	Alchalbi et al. (2009)
RAJO	36.681	36.664	−7.2	12.5	0.5	0.5	0.019	Alchalbi et al. (2009)
RSHM	35.769	35.659	−6.1	11.9	0.5	0.5	0.009	Alchalbi et al. (2009)
SALM	36.966	35.049	−3.6	14.4	0.4	0.4	0.000	Alchalbi et al. (2009)
AYVA	26.707	39.326	−21.1	−9.8	0.7	0.7	−0.009	Reilinger et al. (2006)
NICO	33.396	35.141	−6.2	3.1	0.5	0.5	0.000	Reilinger et al. (2006)
MERS	34.256	36.566	−11.6	4.9	0.7	0.7	0.000	Reilinger et al. (2006)
MER0	34.552	36.900	−12.2	4.4	1.1	1.0	0.029	Reilinger et al. (2006)
ULCN	35.870	36.397	−5.4	9.5	1.7	1.6	−0.001	Reilinger et al. (2006)
ULUC	35.940	36.456	−9.6	9.7	1.0	1.0	0.003	Reilinger et al. (2006)
SENK	36.131	36.050	−5.1	10.2	0.7	0.6	−0.015	Reilinger et al. (2006)
DORT	36.137	36.899	−11.1	9.6	0.5	0.5	−0.012	Reilinger et al. (2006)
ISKE	36.180	36.540	−9.9	12.2	1.7	1.8	−0.033	Reilinger et al. (2006)
PNLR	36.245	38.231	−13.8	8.4	1.6	1.4	−0.016	Reilinger et al. (2006)
ANDR	36.330	37.572	−14.1	8.9	1.7	1.6	−0.031	Reilinger et al. (2006)
ABAK	36.465	36.531	−7.4	11.9	0.9	0.8	0.007	Reilinger et al. (2006)
HASA	36.524	36.788	−7.8	10.1	0.7	0.7	−0.004	Reilinger et al. (2006)
FEVZ	36.643	37.088	−7.5	11.0	0.8	0.7	−0.016	Reilinger et al. (2006)
SAKZ	36.972	37.190	−8.2	11.6	0.5	0.5	−0.009	Reilinger et al. (2006)
KMAR	36.996	37.522	−9.4	10.6	0.6	0.6	−0.020	Reilinger et al. (2006)
KILI	37.106	36.685	−8.0	10.5	1.8	1.7	−0.060	Reilinger et al. (2006)
ABEY	37.113	37.747	−12.0	8.3	0.7	0.7	−0.011	Reilinger et al. (2006)
ELBI	37.220	38.179	−13.2	9.4	0.7	0.7	−0.017	Reilinger et al. (2006)
ALAR	37.436	37.518	−7.4	11.5	0.7	0.7	−0.014	Reilinger et al. (2006)
GAZI	37.574	36.901	−6.7	13.7	0.6	0.5	−0.012	Reilinger et al. (2006)
ALTP	37.869	38.050	−13.3	9.7	0.7	0.7	−0.014	Reilinger et al. (2006)
CKRH	37.886	37.541	−7.1	12.6	0.7	0.7	−0.011	Reilinger et al. (2006)
ARGA	37.902	37.237	−6.8	13.6	0.7	0.7	−0.021	Reilinger et al. (2006)
MLTY	38.215	38.456	−11.5	10.9	0.7	0.7	−0.012	Reilinger et al. (2006)

Table 2 (*Continued*)

Site	Lon. (°)	Lat. (°)	v_e (mm/yr)	v_n (mm/yr)	σ_{Ve} (mm/yr)	σ_{Vn} (mm/yr)	ρ_{VeVn}	Source
MLT1	38.215	38.456	−11.5	10.9	0.7	0.7	−0.012	Reilinger et al. (2006)
ADYI	38.231	37.747	−7.6	14.1	0.8	0.8	−0.002	Reilinger et al. (2006)
GMKV	39.254	38.640	−13.6	10.9	1.2	1.2	−0.046	Reilinger et al. (2006)
TUNC	39.524	39.071	−17.0	12.0	1.5	1.3	−0.004	Reilinger et al. (2006)
KRCD	39.805	37.847	−8.9	15.1	0.8	0.7	−0.006	Reilinger et al. (2006)
KAKO	40.052	38.963	−13.5	9.9	1.6	1.4	−0.012	Reilinger et al. (2006)
KIZ2	40.650	37.246	−6.4	16.6	0.8	0.8	−0.023	Reilinger et al. (2006)
KIZI	40.651	37.247	−6.4	16.6	0.8	0.8	−0.023	Reilinger et al. (2006)
SOLH	41.057	38.959	−6.8	11.5	1.4	1.2	−0.024	Reilinger et al. (2006)
VART	41.454	39.186	−5.9	10.7	2.0	1.3	−0.046	Reilinger et al. (2006)
KRKT	41.794	38.754	−4.7	14.8	0.8	0.7	0.107	Reilinger et al. (2006)
SRNK	42.457	37.528	−6.5	15.1	2.7	1.2	0.042	Reilinger et al. (2006)
RESD	42.547	38.488	−5.6	14.0	1.5	1.2	−0.045	Reilinger et al. (2006)
KAL2	43.341	38.549	−5.1	13.1	0.9	0.8	0.014	Reilinger et al. (2006)
KHAS	56.233	26.208	3.9	24.8	1.5	1.2	0.014	Reilinger et al. (2006)
KALL	43.335	38.506	−9.2	13.7	1.6	1.7	−0.190	New Survey
BLNK	42.314	39.067	−1.2	10.1	0.6	0.7	−0.130	New Survey
BTLS	42.120	38.419	−7.6	14.8	2.1	2.2	−0.160	New Survey
IDIL	41.843	37.350	−9.0	17.7	2.4	2.4	−0.160	New Survey
KZLK	41.504	38.182	−7.0	19.1	2.2	2.3	−0.200	New Survey
VART	41.454	39.186	−4.6	10.2	0.8	0.8	−0.030	New Survey
SOLH	41.057	38.959	−5.9	12.9	0.8	0.9	−0.140	New Survey
SAVR	40.878	37.550	−10.5	17.8	3.0	1.9	−0.200	New Survey
GENC	40.575	38.758	−7.9	20.5	1.6	1.3	−0.100	New Survey
KIGI	40.365	39.324	−10.0	6.6	1.1	1.2	−0.160	New Survey
KAKO	40.052	38.963	−18.3	11.2	1.1	0.9	−0.100	New Survey
HISA	39.835	37.526	−12.6	10.9	1.8	2.2	−0.090	New Survey
AYZC	39.417	36.971	−10.6	14.6	1.5	1.6	−0.080	New Survey
CUNG	39.299	38.207	−10.7	10.1	1.5	1.8	−0.060	New Survey
GMKV	39.254	38.640	−17.0	11.0	0.7	0.7	−0.120	New Survey
CMGZ	38.922	39.059	−23.3	9.2	0.5	0.5	−0.090	New Survey
AKMA	38.400	37.178	−8.7	13.8	0.8	0.8	−0.120	New Survey
AKAB	36.599	36.737	−9.0	11.0	0.8	1.0	−0.130	New Survey
SERI	36.216	36.379	−4.7	9.6	1.4	1.8	−0.030	New Survey
ISKE	36.180	36.540	−8.1	9.8	0.8	1.0	−0.060	New Survey
NICO	33.396	35.141	−5.0	1.3	0.2	0.2	−0.060	New Survey
SEMD	44.574	37.305	−4.1	18.0	0.6	0.7	0.068	CORS Stations
BASK	44.017	38.044	−2.9	15.7	0.1	0.1	−0.061	CORS Stations
OZAL	43.989	38.657	−0.9	15.5	0.8	0.1	−0.008	CORS Stations
CATK	43.061	38.007	−1.8	13.1	0.9	0.1	−0.009	CORS Stations
SIRN	42.457	37.525	−6.1	11.2	0.5	0.1	−0.017	CORS Stations
TVAN	42.291	38.530	−2.4	15.7	0.9	0.1	−0.030	CORS Stations
SIRT	41.936	37.932	−4.4	15.5	0.5	0.6	−0.039	CORS Stations
MUUS	41.502	38.793	−12.8	16.1	0.4	0.4	−0.023	CORS Stations
MIDY	41.357	37.417	−4.8	15.2	0.4	0.4	−0.018	CORS Stations
BTMN	41.155	37.864	−5.4	15.4	0.3	0.4	−0.022	CORS Stations
DIYB	40.188	37.954	−6.6	17.2	0.1	0.1	0.006	CORS Stations
ERGN	39.758	38.270	−6.6	14.9	0.4	0.4	−0.013	CORS Stations
VIRA	39.751	37.234	−5.6	14.6	0.5	0.5	−0.013	CORS Stations
TNCE	39.546	39.110	−14.4	9.4	0.4	0.4	−0.060	CORS Stations
SIVE	39.329	37.752	−6.1	14.1	0.4	0.5	−0.028	CORS Stations
ELAZ	39.257	38.645	−15.0	10.8	0.4	0.4	−0.024	CORS Stations
SURF	38.818	37.192	−8.2	14.3	0.3	0.3	−0.031	CORS Stations
ARPK	38.487	39.041	−14.5	9.9	0.4	0.4	−0.029	CORS Stations
ADIY	38.230	37.746	−5.7	13.0	0.3	0.3	−0.035	CORS Stations
MALY	38.217	38.338	−12.1	10.8	0.3	0.4	−0.028	CORS Stations
DIVR	38.104	39.394	−14.8	9.7	0.5	0.6	−0.019	CORS Stations
ANTE	37.374	37.065	−5.2	12.7	0.3	0.3	−0.031	CORS Stations
GURU	37.308	38.717	−13.6	8.7	0.4	0.4	−0.024	CORS Stations
EKIZ	37.188	38.059	−13.4	8.9	0.4	0.5	−0.030	CORS Stations
KLIS	37.112	36.709	−5.2	12.1	0.4	0.4	−0.029	CORS Stations
MARA	36.931	37.581	−9.9	9.2	0.7	0.7	−0.014	CORS Stations
ONIY	36.254	37.102	−10.5	7.8	0.4	0.4	−0.036	CORS Stations
TUFA	36.221	38.261	−13.0	6.9	0.4	0.4	−0.025	CORS Stations
FEEK	35.912	37.815	−12.1	7.1	0.4	0.5	−0.016	CORS Stations
ADAN	35.344	37.004	−8.0	5.3	0.4	0.4	−0.037	CORS Stations
MRSI	34.603	36.781	−10.9	3.6	0.4	0.4	−0.039	CORS Stations
DIPK	34.195	35.537	−6.6	4.2	0.8	0.8	−0.020	CORS Stations
SILF	33.936	36.382	−8.8	2.3	0.4	0.0	−0.031	CORS Stations
LEFK	33.353	35.195	−5.3	3.3	0.5	0.5	−0.022	CORS Stations

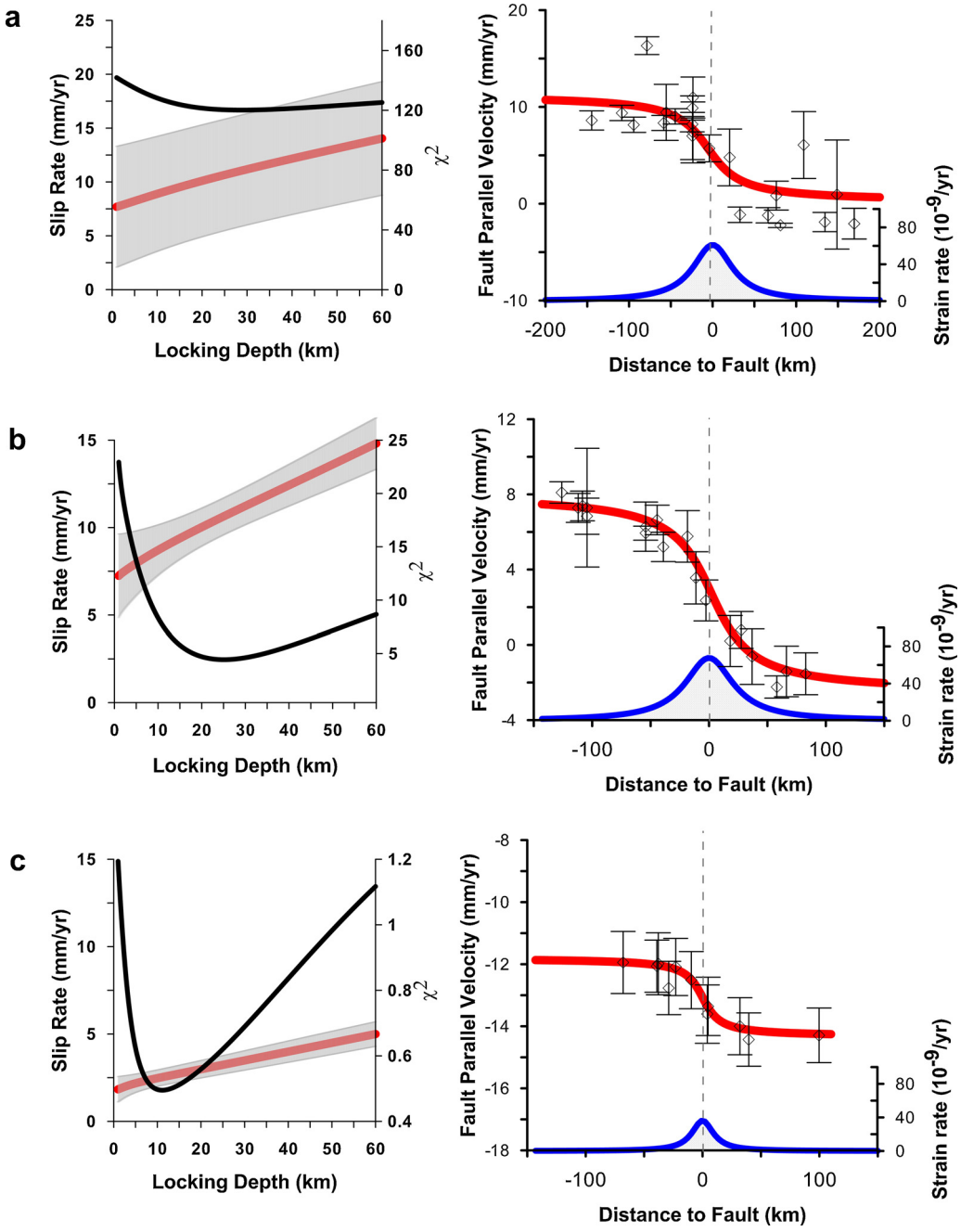

Fig. 3. The variability of the slip rates w.r.t. the locking depth (red) and the χ^2 values of the estimation (black). The thick gray bands show 2-σ error bounds of the slip rates for profiles a to c (left panel) and the velocity profiles with slip rate and locking depth estimated simultaneously (right panel). The red curve shows the model fit to the GPS data (open circles with error bars at 95% confidence level) and the blue curve is the fault parallel shear strain rate for the best fit model determined from the analysis shown in Fig. 3 and described in the text. (For interpretation of the references to color in this figure legend, the reader is referred to the web version of the article.)

that profile. The difficulty of estimating the locking depth in that profile has been addressed by Alchalbi et al. (2009). Our estimate of locking depth (11.3 ± 6.7 km) is close agreement with the estimate of Le Beon et al. (2008) for DSFS. The velocity profiles with the estimated slip rates and locking depths are also shown in Fig. 3.

3.3. Block modeling and slip rates

The estimation of slip rates from a sparse set of observations is highly sensitive to block discretization, the assumed locking depths, and the spatial density of data. The lack of sufficient data near block boundaries and, at the same time, within the rigid parts of the blocks, usually results in a high correlation of parameters, such that the elastic strain accumulation cannot be distinguished rigorously from the rigid block rotations. Moreover, the trade-off between slip rate and locking depth largely depends on the network coverage and the spatial density. Even if we assume that the slip rate of the EAFS is constant across all its individual segments, the accumulation and the release of strain still depend on the variation of the locking depth. In this respect, rigorous determination of slip rates and locking depths is also important for hazard studies.

To investigate the slip rate variation along the EAFS and to determine how much of the deformation can be explained with rigid blocks, we formed a block model which extends from Karliova in the north and Cyprus Island in the south. We employed an approach similar to that of McCaffrey (2002), where all the Euler

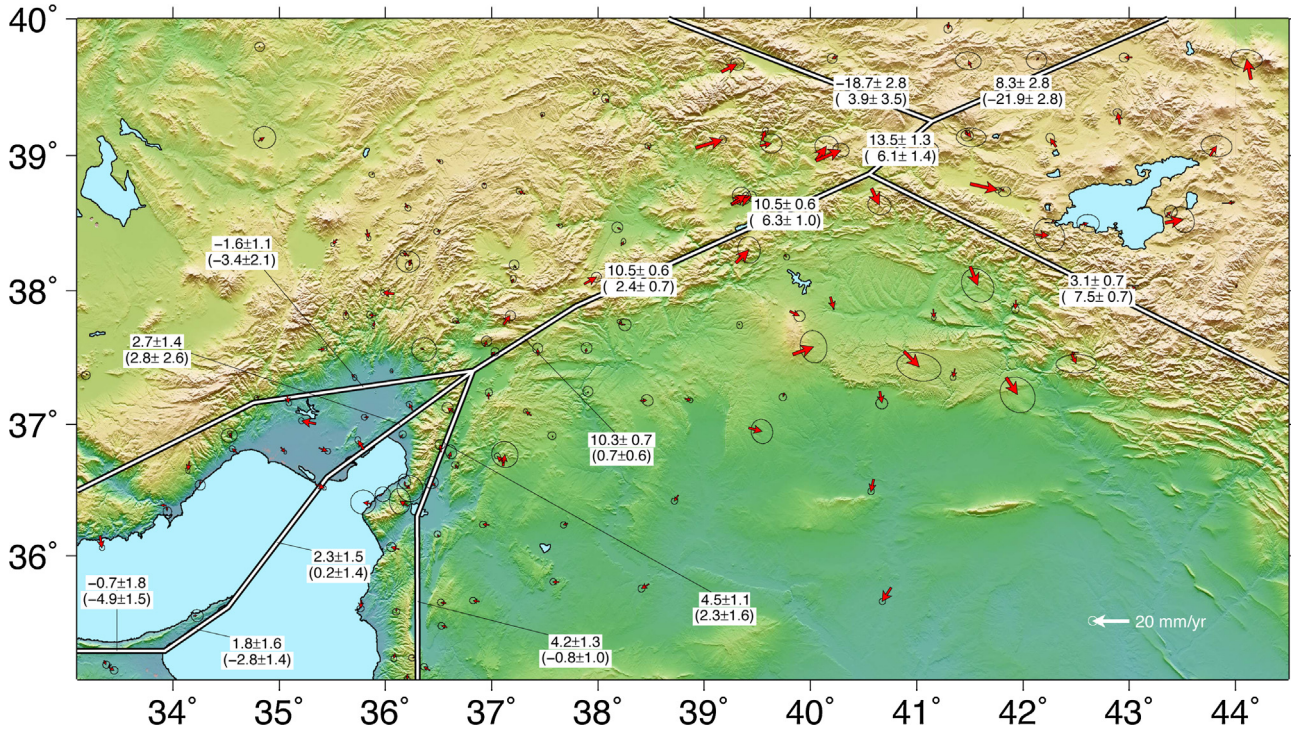

Fig. 4. The slip rates obtained from the block modeling and the residual velocity field. The values at the top (without parenthesis) show the fault parallel slip rates in which the positive and negative values correspond to left and right lateral slip rates, respectively. The values at the bottom (in parenthesis) show the fault normal slip rates in which the positive and negative values correspond to the contraction and the extension rates, respectively.

rotations of the micro blocks are simultaneously estimated by minimizing the misfit of the velocities. The back-slip model given in Matsu'ura et al. (1986) was also applied to each fault segment to mimic elastic strain accumulation during the interseismic phase of the earthquake cycle. The elastic strain along the block boundaries was computed by using the analytical equations given in Okada (1985). The block velocities estimated in the form of Euler vectors were then used to determine the fault slip rates in the middle of the each segment. Since the segment lengths vary from one to a few hundreds kilometers, the spatial resolution of the estimated slip rates are also variable. It should also be noted that the slip rates on multiple consecutive segments bordering two large blocks do not vary unless there is no sharp change in the geometry of segments. The block boundaries are shown in Fig. 4, and are consistent with the Active Fault Map of Turkey (Şaroğlu et al., 1992b). Following the findings in the previous section, the locking depths of the block boundaries were taken as 25 km except for the southern continuation of the EAFS toward DSFS and Cyprus Arc, where they were assumed to be 12 km. A dip angle of 45° was assumed for the thrusting parts of EAFS and 90° for strike-slip segments.

While there is a certain trade-off in the simultaneous estimation slip rates and locking depth from velocity profiles, the slip rates estimated in block models are mainly controlled by the relative block motion. The effect of elastic back-slip is limited to sites close to the fault zone (2–3 times the locking depth). For small blocks with most sites are very close (within the distance of 2–3 times the locking depth) to the fault zone, the effect of pre-defined locking depth in block models results could be dramatic. For large blocks with sufficient number of sites far from the fault zone, the effect of locking depth on the slip rates could be insignificant in block modeling since the relative motion of the block is then mostly determined by the relative motion of far field sites. To investigate the effect of locking depth, several different extreme and moderate values for the EAFS segments were taken into account. At the lower extreme, assuming a locking depth of 10 km for all the segments along the EAFS, the block model produces a normalized rms (nrms) of 22.00, while at the higher extreme, assuming 25 km for all the segments along the EAFS produces a nrms of 21.76. For a moderate value of 15 km, the locking depth for all the segments along the EAFS gives a nrms of 21.79. Assuming 12 km locking depths for southern segments and 25 km for northern segments gives a nrms of 22.07. In terms of weighted rms, the differences between different values of locking depths are within 0.5 mm/yr. The differences are insignificant to favor one set of locking depths over another. In this respect, we believe that the slip rates in our block model are insensitive to the choice of locking depth within the data error bounds.

The slip rate estimates computed from velocity profiles for the profiles (a) and (b) are 11.06 ± 3.94 and 10.65 ± 0.92 (Table 3) and are statistically the same and indistinguishable. The slip rate estimates from block modeling (10.5 ± 0.6) for the same segments are also in agreement with those computed from the velocity profiles and confirms a constant slip rate of 10–11 mm/yr for the part of the EAFS in the north of Türkoğlu (Fig. 2). While the left-lateral slip rate in the northern part of the EAFS near Karliova seems to be larger (~13 mm/yr) in the block modeling (Fig. 4) than the middle segments, the difference between them is not statistically significant at 95% confidence level. Furthermore, this northernmost segment is relatively short and possibly not well constrained by the available data. On the other hand, the southernmost segment of the EAFS (to the south of Türkoğlu) was found to have a significantly

Table 3
The simultaneous estimation of the slip rates and the locking depth. The results of the simultaneous estimation of the profile parameters D (depth) and V (slip rate) in Eq. (2) and associated one-sigma uncertainties.

	D (km)	V (mm/yr)
a	28.85 ± 29.24	11.06 ± 3.94
b	25.08 ± 6.25	10.65 ± 0.92
c	11.13 ± 6.73	2.53 ± 0.41

lower left-lateral slip rate of 4.5 ± 1.1 mm/yr in the block modeling. The slip rate was found to be ~4 mm/yr on the northern part of the DSFS. Similarly, the contraction rates of ~6 mm/yr near Karliova and becomes insignificant in the southern segments of the EAFS. The contraction rates which are only available from the block modeling show a contrast between the northern (6.1–6.3 mm/yr) and southern (0.7–2.4 mm/yr).

4. Results and discussion

There is no global plate motion model in the literature which documents a slip rate for the Anatolia-Arabia boundary to directly compare with those estimated using GPS data. The global plate motion models, in which an Arabia–Eurasia convergence rate is available, show that the GPS-based estimates of the convergence rate of the Arabia–Eurasia collision is usually slower than the corresponding estimates of plate circuit models (DeMets et al., 1990, 1994; Sella et al., 2002). In earlier studies, the relative motion between the Arabian and the Anatolian plates was estimated through regional GPS networks, and the GPS-based estimates show a slip rate of 11 mm/yr based on the relative rotations of these large blocks (Reilinger et al., 1997; McClusky et al., 2000). Based on block modeling, Reilinger et al. (2006) reported left lateral slip rates of 9.9 ± 0.2 mm/yr and 10.0 ± 0.3 mm/yr along with contraction rates of 5.1 ± 0.3 mm/yr and 2.9 ± 0.3/yr for the northern part of the EAFS. They also found slower left-lateral slip rates (5.5–6.8 mm/yr) and faster contraction rates (6.4–7.9 mm/yr) on the continuation of the EAFS to the Dead Sea Fault System (DSFS). Mahmoud et al. (2013) reported a constant slip rate of 9.7 ± 0.9 mm/yr for the whole EAFS.

We found that the left-lateral slip rate along the EAFS drastically changes from a nearly constant value of ~10 mm/yr in the north to 4.5 mm/yr to the south of Türkoğlu. The Çelikhan-Gölbaşı segment, which lies to the north of a triple junction (see Fig. 4), has a left-lateral slip rate of ~10 mm/yr. While our estimates of left-lateral slip rate are in general agreement with the earlier studies, our denser data set and assumed block geometry allow us to constrain the slip rates of the individual segments of the EAFS, and does not require the assumption of a constant slip rate assumption along the entire EAFS. The variation of the slip rate along a major strike-slip fault system has also been noted by different researchers for the case of the DSFS. While a generalized block model shows a uniform slip rate of 4.5 ± 0.3 mm/yr for the DSFS (Reilinger et al., 2006), more recent and denser GPS networks reveal a gradual variation between 4.5 mm/yr along the southern segment (Mahmoud et al., 2013) and 2 mm/yr along the northern segment (Alchalbi et al., 2009). The determination of slip rates through the differential rotation of blocks involves the assumption of a constant slip rate along a specific fault zone. However, the slip rates along a long fault system can vary depending on elasticity variations even if the driving velocity is constant (Chéry, 2008). Another difficulty in the estimation of slip rates only through relative block rotations arises from the necessity of using a set of GPS sites within the rigid part of the plate. For instance, Aktuğ et al. (2013) quantify the obvious westward increase of GPS velocities within Central Anatolia, which was often assumed rigid in earlier studies (McClusky et al., 2000; Reilinger et al., 2006). Furthermore, the projection of the estimated small circle along the fault does not take account of actual departure of the fault orientation from the small circle and the consequent fault-normal slip (contraction/extension) (Oral et al., 1995; Reilinger et al., 1997; McClusky et al., 2000). In this respect, the estimates of early GPS studies (9–11 mm/yr) could represent an average value of the slip rate along a long fault segment. One way to deal with these difficulties is to discretize the fault boundary and take the elastic strain accumulation into account. In those models, the slip rates along the faults are estimated through differential rotation of bounding blocks while the elastic strain accumulation along block boundaries is also taken into account (McCaffrey, 2002). More recent GPS studies (i.e. Reilinger et al., 2006), which employ such methodology, give slip rates similar to the earlier estimates of ~10 mm/yr (Oral et al., 1995; Reilinger et al., 1997). However, such a model is also highly sensitive to block discretization. In addition, a dense and spatially uniform distribution of GPS sites is needed to distinguish the rigid block rotation from the elastic deformation. In this respect, we believe that the most reliable estimate of slip rates and its variation along the EAFS has been possible using the more complete data set presented in this study.

Our estimate of slip rate for the segment between Karlıova and Çelikhan is higher than the 4 mm/yr that is reported in Aksoy et al. (2007) based on the total geological offset of Lake Hazard but in good agreement with the geological slip rate of 8.3 mm/yr given in Herece (2008). In a more recent study, Karabacak et al. (2010) found a well-constrained slip rate of 4.94 ± 0.13 mm/yr for the northern part of the DSFZ based on the offset of a pre-Quaternary basin. Meghraoui et al. (2003) used well-constrained historical evidence to estimate a slip rate of 6.9 ± 0.1 mm/yr at northwestern Syria along the DSFS. Sbeinati et al. (2010) proposed a slip rate of 4.9–6.3 mm/yr based on archaeoseismology data in the northern part of the DSFS. All these are also in good agreement with our GPS estimate (4.5 ± 1.1 mm/yr) for the same segment. The slip rate estimates from both profile and block models are 2.53 ± 0.41 and 4.2 ± 1.3 mm/yr, respectively. For a confidence level of 95%, our block model estimate lies within an interval between 1.6 mm/yr and 6.8 mm/yr, which is consistent both with our estimate of the profile velocity and the estimate of 2 mm/yr given in Alchalbi et al. (2009). The agreement of our estimates with the one given in Alchalbi et al. (2009) is expected since our new data only covers the northern part of the study area and our modeling results relies on the data given in Alchalbi et al. (2009) for the northernmost segment on the DSFS.

There are three continuous GPS stations in our data set, which are located on Cyprus. While the LEFK and NICO (IGS) stations are in the south, the DIPK station is north of the Cyprian Arc (Fig. 2). Although they are from different sources, the difference in the north velocities of LEFK and NICO is about ~0.2 mm/yr, which is well below the uncertainty of the estimates. The difference between the north–south velocities of DIPK and NICO-LEFK is ~1 mm/yr and no significant difference is observed between the east–west velocities. While geomorphologically distinct, our GPS estimates do not show any significant motion across the border of the Cyprian Arc lying in Cyprus Island. Similarly, very low subduction rates are reported for the Cyprian Arc with respect to the Hellenic Arc, based on the observed minor shortening of the Quaternary sediments (Doglioni et al., 2002). On the other hand, as shown in our block modeling (Fig. 4), extension rates of up to 3.5 mm/yr were observed between the southernmost coast of Anatolia and the south coast of Cyprus.

Our profile analysis also reveals the variation in locking depth from a very high value of 25.08 ± 6.25 km along the EAFS in the north to 11.13 ± 6.73 km along the DSFS in the south, corresponding to a difference of 13.95 ± 9.18 km. While such a difference seems to be large, it is only significant at 87% confidence level. In this respect, our data cannot reliably distinguish any possible variation of the locking depth between the northern and southern profiles. The simultaneous determination of slip rate and locking depth in the new northern profile (profile a in Fig. 3) is not reliable with large uncertainty in locking depth (Table 3). On the other hand, the slip rate is nearly constant when it is estimated for a constant locking depth (Fig. 3, upper left panel) and found to be statistically the same as profile (b). Similarly, fault parallel velocities of profile (a) are in general inconsistent with the velocity curve in Savage–Burford model (Fig. 3). This could be due to the fact that the deformation in that part of the domain is too complex to fit into a simple strike-slip model. While the northern profile is well-constrained by the

spatial density of our data, the southern profile is not, due to the density of data on the western side of the profile. The difficulty of estimating locking depth on this profile has also been addressed by Alchalbi et al. (2009) and Mahmoud et al. (2013). However, Le Beon et al. (2008) found a locking depth of 11 ± 9 km in the southern part of the DSFS using a different data set and methodology, which is in close agreement with our estimate of 11.1 ± 6.7 km. The slip rates from recent InSAR studies on the northernmost segment of the EAFS range between 11 ± 3 mm/yr (Walters et al., 2014) and 13 mm/yr (Cavalié and Jónsson, 2014), in close agreement with our estimate of 10.5 mm/yr.

The segmentation of the EAFS in the literature varies widely. The slip rate estimates by the block modeling are independent of the segmentation as long as no abrupt change is assumed in the geometry of the faults. Such well-known fault-end effect could also emerge from abrupt changes in locking depth or dip angle. On the other hand, the Anatolia and Arabian blocks on either side of the EAFS in our model are large blocks with a sufficient number of sites far from the fault zone to minimize the possible fault end effect on the estimated slip rates.

We assumed a common and simple segmentation scheme for easy discretization and computation of the slip rates. However, the slip rates for other segmentations can be inferred from the given estimates of slip rates. While our block discretization in this paper is consistent with the most recent active fault map of Turkey, it should be noted that the results of the block modeling are, in general, sensitive to block definition. Due to its complex geometry, the segmentation of the EAFS and the exact location of the triple junction of African, Arabian and Anatolian plates near the EAFS are still disputed (Barka and Kadinsky-Cade, 1988; Şaroğlu et al., 1992a; Hempton et al., 1981; Herece, 2008; Duman and Emre, 2013). In this respect, different block geometries are also possible and the slip rate estimates could change drastically depending on the employed block definition.

The exact locations of historical 1874 (M:7.1) and 1875 (M:6.7) earthquakes are still under dispute. While Ambraseys and Jackson (1998) and Çetin et al. (2003) suggested that the 1874–1875 earthquakes occurred between Sivrice and Palu, Nalbant et al. (2002) and Herece (2008) asserted that they occurred on the segment between Sivrice and Sincik. A recent detailed study in the region also supports the idea that the 1874 (M:7.1) and 1875 (M: 6.7) earthquakes took place between Sivrice and Palu (Duman and Emre, 2013). There is no other historical evidence for large earthquakes between Sivrice and Palu, which lie on the 135-km long Palu-Sincik segment. The largest earthquake between Sivrice and Sincik is the 1905 (M:6.8) earthquake, which is considered to occur outside the main EAFS zone (Duman and Emre, 2013). In both cases, our slip rate estimates for both segments are the same (10.5 mm/yr). Such high slip rates for the whole Palu-Sincik segment corresponds to a slip deficit of 1.5 m since 1875 and a potential M_w7.4 earthquake. Çetin et al. (2003) suggested a recurrence interval of 360 years for the Palu-Sivrice segment, based on the offset of the 1874 earthquake, and a slip rate of 11 mm/yr. Duman and Emre (2013) also estimated a recurrence interval of this segment as 350–400 years, based on GPS-derived slip rates and the geological offsets of 1874 earthquake.

Apart from the 1893 (M:7.1) earthquake which occurred near Çelikhan (Fig. 1) (Ambraseys, 1989; Ambraseys and Jackson, 1998), no large historical earthquake has been reported between Çelikhan and Türkoğlu. The most recent significant earthquake (M:7.4) on the Gölbaşı-Türkoğlu segment is reported to have occurred in 1513 (M:6.7) (Ambraseys, 1989). Another earthquake dated as 1114 was also reported in this segment using paleoseismological results (Meghraoui et al., 2006; Karabacak et al., 2010). Such observations imply a recurrence interval of ~400 years. Duman and Emre (2013) also suggested a recurrence interval of 400–500 years using a slip rate of 6.5–7.0 mm/yr. In this respect, our estimate of 10.3 ± 0.7 mm/yr for this segment corresponds to a shorter recurrence interval (260–330 years) for an earthquake with the same magnitude (M:6.7) or a larger earthquake with a longer recurrence interval. The cumulative slip deficit since 1513 corresponds to 5.2 m with a slip rate of 10.3 mm/yr. Even if we assume that the 1893 (M:7.1) earthquake occurred within the Çelikhan-Gölbaşı segment, the Gölbaşı-Türkoğlu segment has a very large seismic potential of M_w7.7 earthquake.

5. Conclusion

Unlike the NAFS, previous GPS studies on the EAFS have used regional scale data and are limited in number. In those studies, it has not been possible to determine slip rates on the different segments of the EAFS due to the sparse distribution of geodetic stations. On the other hand, the relatively quiet EAFS has been known to produce large earthquake during historic times (Ambraseys, 1989). Therefore, estimating fault slip rates on the EAFS and determining its seismic potential is important. In this study we determine fault slip rates on the EAFS with geodetic observations of high spatial resolution, better geometric configuration and higher precision. The left lateral slip rates of the EAFS are significantly different between the parts to the north and to the south of Türkoğlu. While the slip rate is nearly constant (~10 mm/yr) in the north, it sharply decreases to 4.5 mm/yr in the south. Such a variation in slip rates is possibly accompanied by a variation in locking depth. Analysis of the profiles of GPS velocities across the EAFS reveals that the locking depth in the northern part of the fault is considerably greater than that to the south. The complex geology and faulting geometry does not permit us to further investigate the variation of the locking depths. The estimate of locking depth in the northernmost profile (profile a) is 28.85 ± 29.24 km, which is far from a reliable estimate. On the other hand, a constant locking depth experiment in the same profile shows that slip rate is nearly independent of the locking depth in that profile. While the locking depth In the middle segment of the EAFS is 25.08 ± 6.25 km, it is only 11.13 ± 6.73 km along the DSFS in the south. However, given the uncertainties, such a variation is not significant at 95% level. The contraction rates along the EAFS are mostly insignificant except for the northern parts and it reaches a maximum value of 6.1 ± 1.4 mm/yr near Karliova. Such low contraction rates between the Arabian and Anatolia plates also support the hypothesis that the pull of the Hellenic Arc is the dominant mechanism in the kinematics of Anatolia. The determination of variations in the slip rate along the EAFS is of critical importance in assessing the seismic potential of two well-known seismic gaps on the EAFS, the Palu-Sincik and Çelikhan-Türkoğlu segments. The largest left-lateral slip rate was found to be 10.5 ± 0.6 mm/yr on the Palu-Sincik segment (Fig. 1). Since the most recent earthquake on this segment occurred in 1875, it has a slip deficit of 1.5 m and has the potential of producing an earthquake of M_w7.4, if the whole segment ruptured in a single event. Higher slip rates found in this seismic gap also shorten the earlier estimates of the recurrence interval from ~400 years to ~300 years. The second seismic gap lies on the segment between Çelikhan and Türkoğlu, which is the best-constrained part in our model. The Çelikhan-Türkoğlu segment shows a left lateral slip rate of 10.3 ± 0.7 mm/yr. Since the most recent earthquake on this segment occurred in 1513, it has a slip deficit of 5.2 m. Even if we assume that the 1893 (M:7.1) earthquake occurred within the Çelikhan-Gölbaşı segment, it still has a very high seismic potential for an event as large as M_w7.7.

Acknowledgments

This project is supported by Boğaziçi University Scientific Research Projects (BAP) under grant 12T03P1. We are grateful to the

many individuals and institutions supporting the collection of data presented here. Part of this work was completed during a sabbatical leave by the first author at Université Montpellier-II, which was supported by the grant B.14.2.TBT.0.06.01-219-84 by The Scientific and Technological Research Council of Turkey (TÜBİTAK). It is also particularly acknowledged that useful criticism and suggestions provided by the editor and two anonymous reviewers improved the content of this paper.

References

Aksoy, E., İncegöz, M., Koçyiğit, A., 2007. Lake Hazar Basin: a negative flower structure on the East Anatolian Fault System (EAFS), SE Turkey. Turk. J. Earth Sci. 16, 319–338.

Aktuğ, B., Lenk, O., Gürdal, M.A., Kilicoglu, A., 2009. Establishment of regional reference frames for detecting active deformation areas in Anatolia. Stud. Geophys. Geod. 2 (53), 169–183.

Aktuğ, B., Parmaksız, E., Kurt, M., Lenk, O., Kılıçoğlu, A., Gürdal, M.A., Özdemir, S., 2013. Deformation of Central Anatolia: GPS implications. J. Geodyn. 67, 78–96.

Alchalbi, A., Daoud, M., Gomez, F., et al., 2009. Crustal deformation in northwestern Arabia from GPS measurements in Syria: slow slip rate along the northern Dead Sea Fault. Geophys. J. Int. 180, 125–135.

Allen, M., Jackson, J., Walker, R., 2004. Late Cenozoic reorganization of the Arabia–Eurasia collision and the comparison of short-term and long-term deformation rates. Tectonics 23 (1), TC2008.

Ambraseys, N.N., 1989. Temporary seismic quiescence: SE Turkey. Geophys. J. Int. 96, 311–331.

Ambraseys, N.N., Jackson, J.A., 1998. Faulting associated with historical and recent earthquakes in the Eastern Mediterranean region. Geophys. J. Int. 133, 390–406.

Arpat, E., Sarağlu, F., 1972. The East Anatolian Fault System: thoughts on its development. Min. Res. Explor. Inst. Turkey Bull. 78, 33–39.

Barka, A.A., Kadinsky-Cade, K., 1988. Strike-slip fault geometry in Turkey and its influence on earthquake activity. Tectonophysics 7, 663–684.

Berberian, M., King, G.C.P., 1981. Towards a paleogeography and tectonic evolution of Iran. Can. J. Earth Sci. 18, 210–265.

Bozkurt, E., 2001. Neotectonics of Turkey – a synthesis. Geodin. Acta 14, 3–30.

Cavalié, O., Jónsson, S., 2014. Block-like plate movements in eastern Anatolia observed by InSAR. Geophys. Res. Lett. 41, 26–31.

Çetin, H., Güneyli, H., Mayer, L., 2003. Paleoseismology of the Palu-Lake Hazar segment of the East Anatolian Fault Zone,Turkey. Tectonophysics 374, 163–197.

Chéry, J., 2008. Geodetic strain across the San Andreas fault reflects elastic plate thickness variations (rather than fault slip rate). Earth Planet. Sci. Lett. 269, 351–364.

DeMets, C., Gordon, R.G., Argus, D.F., Stein, S., 1990. Current plate motions. Geophys. J. Int. 101, 425–478.

DeMets, C., Gordon, R.G., Argus, D.F., Stein, S., 1994. Effects of recent revisions to the geomagnetic reversal time scale on estimates of current plate motions. Geophys. Res. Lett., 2191–2194.

Dewey, J.F., Hempton, M.R., Kidd, W.S.F., Şaroğlu, F., Şengör, A.M.C., 1986. Shortening of continental lithosphere: the neotectonics of eastern Anatolia: a young collision zone. In: Coward, M.P., Ries, A.C. (Eds.), Collision Tectonics. Geol. Soc. Lond. Spec. Publ. 19, 3–36.

Doglioni, C., Agostini, S., Crespi, M., Innocenti, F., Manetti, P., Riguzzi, F., Savascin, Y., 2002. India–Asia convergence in NW Himalaya. In: Rosenbaum, G., Lister, G.S. (Eds.), Reconstruction of the Evolution of the Alpine-Himalayan Orogen. J. Virtual Explor. 7, 167–181.

Dong, D., Herring, T.A., King, R.W., 1998. Estimating regional deformation from a combination of space and terrestrial data. J. Geod. 72, 200–211.

Duman, T.Y., Emre, Ö., 2013. The East Anatolian Fault: geometry, segmentation and jog characteristics. Geol. Soc. Lond. Spec. Publ. 372.

GCM, 2013. Velocity Field of Turkish National Permanent GPS Network-Active, General Command of Mapping, Ankara, Turkey. http://www.hgk.msb.gov.tr.

Gök, R., Pasyanos, M., Zor, E., 2007. Lithospheric structure of the continent–continent collision zone: eastern Turkey. Geophys. J. Int. 169, 1079–1088.

Hempton, M.R., 1987. Constraints on Arabian plate motion and extensional history of the Red Sea. Tectonics 6, 687–705.

Hempton, M.R., Dewey, J.F., Şaroğlu, F., 1981. The East Anatolian transform fault: along strike variations in geometry and behaviour. EOS Trans. 62, 393.

Hempton, M.R., 1985. Structure and deformation history of the Bitlis sture near Lake Hazar, southeastern Turkey. Geol. Soc. Am. Bull. 96, 233–243.

Herece, E., Akay, E., 1992. Karlıova-Çelikhan arasında Doğu Anadolu Fayı. In: Proceeding of the 9th Petroleum Congress of Turkey, Ankara, Turkey, 17–21 February 1992, pp. 361–372.

Herece, E., 2008. Doğu Anadolu Fayı (DAF) Atlası, General Directorate of Mineral Research and Exploration, Special Publications, Ankara, Serial Number, 13., pp. 359.

Herring, T.A., 1997. GAMIT/GLOBK Kalman Filter VLBI and GPS Analysis Program; Version 4.1. Massachusetts Institute of Technology, Cambridge.

Jackson, J.A., McKenzie, D.P., 1988. Rates of active deformation in the Aegean Sea and surrounding regions. Basin Res., 121–128.

Jackson, J., McKenzie, D.P., 1984. Active tectonics of the Alpine-Himalayan belt between western Turkey and Pakistan. Geophys. J. R. Astron. Soc. 77, 185–264.

Jaffey, N., Robertson, A.H.F., 2001. New sedimentological and structural data from the Ecemis Fault Zone, southern Turkey: implications for its timing and offset and the Cenozoic tectonic escape of Anatolia. J. Geol. Soc. Lond. 158, 367–378.

Kalafat, D., Kekovalı, K., Güneş, Y., Yılmazer, M., Kara, M., Deniz, P., Berberoğlu, M., 2009. Türkiye ve Çevresi Faylanma-Kaynak Parametreleri (MT) Kataloğu (1938–2008): A Cataloque of Source Parameters of Moderate and Strong Earthquakes for Turkey and its Surrounding Area (1938–2008). Boğaziçi University Publication No=1026, Bebek-İstanbul, 43 pp.

Karabacak, V., Altunel, E., Meghraoui, M., Akyüz, H.S., 2010. Field evidences from northern Dead Sea Fault Zone (South Turkey): new findings for the initiation age and slip rate. Tectonophysics 480, 172–182.

King, R.W., McClusky, S., Herring, T., 2009. Documentation of the GAMIT GPS Analysis Software, Release 10.3. Mass. Inst. of Technol., Cambridge.

Le Beon, M.L., Klinger, Y., Amrat, A.Q., Agnon, A., Dorbath, L., Baer, G., Ruegg, J.-C., Charade, O., Mayyas, O., 2008. Slip rate and locking depth from GPS profiles across the southern Dead Sea Transform. J. Geophys. Res. 113 (B11), B11403.

Lybéris, N., Yürür, T., Chorowicz, J., Kasapoğlu, E., Gündoğdu, N., 1992. The East Anatolian fault: an oblique collisional belt. Tectonophysics 204, 1–15.

Mahmoud, Y., Masson, F., Meghraoui, M., Cakir, Z., Alchalbi, A., Yavasoglu, H., Yönlü, O., Daoud, M., Ergintav, S., Inan, S., 2013. Kinematic study at the junction of the East Anatolian fault and the Dead Sea fault from GPS measurements. J. Geodyn. 67, 30–39.

Matsu'ura, M., Jackson, D.D., Cheng, A., 1986. Dislocation model for aseismic crustal deformation at Hollister, California. J. Geophys. Res. 91 (B12), 2661–2674.

McCaffrey, R., 2002. Crustal block rotations and plate coupling. In: Stein, S., Freymueller, J.T. (Eds.), Plate Boundary Zones: Geodynamics Series, vol. 30. American Geophysical Union, pp. 101–122, http://dx.doi.org/10.1029/030GD06.

McClusky, S., et al., 2000. Global positioning system constraints on plate kinematics and dynamics in the eastern Mediterranean and Caucasus. J. Geophys. Res. 105 (B3), 5695–5719.

McKenzie, D.P., 1970. Plate tectonics of the Mediterranean region. Nature 220, 239–343.

McKenzie, D.P., 1972. Active tectonics of the Mediterranean region. Geophys. J. R. Astron. Soc. 30, 109–185.

Meghraoui, M., Bertrand, S., Karabacak, V., Ferry, M., Cakir, Z., Altunel, E., 2006. Surface ruptures along the Maras segment of the East Anatolian Fault (SE Turkey) and kinematic modelling from Tectonic and GPS data. Geophys. Res. Abstr. 8, 10006, SRef-ID: 1607-7962/gra/EGU06-A-10006.

Meghraoui, M., Gomez, F., Sbeinati, R., Van der Woerd, J., Mouty, M., Darkal, A., Radwan, Y., Layyous, I., Najjar, H.M., Darawcheh, R., Hijazi, F., Al-Ghazzi, R., Barazangi, M., 2003. Evidence for 830 years of seismic quiescence from paleoseismology, archeoseismology and historical seismicity along the Dead Sea fault in Syria. Earth Planet. Sci. Lett. 210, 35–52.

Nalbant, S., McCloskey, J., Steacy, S., Barka, A., 2002. Stress accumulation and increased seismic risk in eastern Turkey. Earth Planet. Sci. Lett. 195 (3–4), 291–298.

Okada, Y., 1985. Surface deformation due shear and tensile faults in a halfspace. Bull. Seismol. Soc. Am. 75, 1135–1154.

Oral, M.B., Reilinger, R.E., Toksöz, M.N., King, R.W., Barka, A., Kınık, İ., Lenk, O., 1995. Global positioning system offers evidence of plate motions in eastern Mediterranean. EOS Trans. 76 (9).

Philip, H., Cisternas, A., Gvishiani, A., Gorshkov, A., 1989. The Caucasus: an actual example of the initial stages of a continental collision. Tectonophysics 161, 1–21.

Reilinger, R.E., McClusky, S., Oral, M.B., King, W., Toksöz, M.N., 1997. Global positioning, system measurements of present-day crustal movements in the Arabian–Africa–Eurasia plate collision zone. J. Geophys. Res. 102, 9983–9999.

Reilinger, R., et al., 2006. GPS constraints on continental deformation in the Africa–Arabia–Eurasia continental collision zone and implications for the dynamics of plate interactions. J. Geophys. Res. 111, B05411.

Robertson, A.H.F., 2000. Mesozoic-tertiary tectonic sedimentary evolution of a south Tethyan oceanic basin and its margins in southern Turkey. In: Bozkurt, E., Winchester, J.A., Piper, J.D.A. (Eds.), Tectonics and Magmatism in Turkey and the Surrounding Area, Geol. Soc. Spec. Publ., No. 173. , pp. 97–138.

Sandvol, E., Turkelli, N., Barazangi, M., 2003. The Eastern Turkey Seismic Experiment: the study of a young continent–continent collision. Geophys. Res. Lett. 30 (24), 8038.

Şaroğlu, F., Emre, Ö., Kuşçu, İ., 1992a. The East Anatolian Fault of Turkey. Ann. Tecton. 6, 125–199.

Şaroğlu, F., Emre, Ö., Kuşçu, İ., 1992b. Turkish Active Faults Map. Directoriate of Mineral Research and Exploration, Ankara, Turkey.

Şaroğlu, F., Emre, Ö., Boray, A., 1987. Türkiye'nin Diri Fayları ve Depremsellikleri, Institute of Mineral Research and Exploration Report, Report no: 8174.

Savage, J., Burford, R., 1973. Geodetic determination of relative plate motion in Central California. J. Geophys. Res. 78, 832–845.

Sbeinati, M.R., Meghraoui, M., Suleyman, G., Gomez, F., Grootes, P., Nadeau, M., Al Najjar, H., Al-Ghazzi, R., 2010. Timing of earthquake ruptures at the Al Harif Roman Aqueduct (Dead Sea fault, Syria) from archeoseismology and paleoseismology, Special volume archaeoseismology and paleoseismology. In: Sintubin, M., Stewart, I.S., Niemi, T.M., Altunel, E. (Eds.), Ancient Earthquakes: Geological Society of America Special Paper 471., http://dx.doi.org/10.1130/2010.2471(20).

Seber, G.A.F., Wild, C.J., 2003. Nonlinear Regression. Wiley-Interscience, Hoboken, NJ.
Segall, P., 2010. Earthquake and Volcano Deformation. Princeton University Press, New Jersey.
Sella, G.F., Dixon, T.H., Mao, A., 2002. REVEL: a model for recent plate velocities from space geodesy. J. Geophys. Res. 107 (B4), 2081.
Şengör, A.M.C., Kidd, W.S.F., 1979. Post-collisional tectonics of the Turkish–Iranian plateau and a comparison with Tibet. Tectonophysics 55, 361–376.
Şengör, A., Görür, N., Şaroğlu, F., 1985. Strike-slip faulting and related basin formation in zones of tectonic escape: Turkey as a case study. In: Biddle, K., Christie-Blick, N. (Eds.), Strike-Slip Deformation, Basin Formation and Sedimentation, Vol. 37. Spec. Publ. SEPM Soc. Sediment. Geol., SEPM, pp. 227–264.
Taymaz, T., Jackson, J., McKenzie, D.P., 1991. Active tectonics of the North and Central Aegean Sea. Geophys. J. Int. 106, 433–490.
Walters, R.J., Parsons, B., Wright, T.J., 2014. Constraining crustal velocity fields with InSAR for Eastern Turkey: limits to the block-like behavior of Eastern Anatolia. J. Geophys. Res. 119, 5215–5234.
Westaway, R., 1994. Present-day kinematics of the Middle East and Eastern Mediterranean. J. Geophys. Res. 99, 12071–12090.
Westaway, R., Arger, J., 1996. The Gölbaşı basin, southeastern Turkey: a complex discontinuity in a major strike-slip fault zone. J. Geol. Soc. Lond. 153, 729–743.
Westaway, R., Arger, J., 2001. Kinematics of the Malatya-Ovacik fault zone. Geodin. Acta 14, 103–131.
Yürür, M.T., Chorowicz, J., 1998. Recent volcanism, tectonics and plate kinematics near the junction of the African, Arabian, and Anatolian plates. J. Volcanol. Geotherm. Res. 85 (1998), 1–15.
Zor, E., Sandvol, E., Gürbüz, C., Türkelli, N., Seber, D., Barazangi, M., 2003. The crustal structure of the East Anatolian plateau (Turkey) from receiver functions. Geophys. Res. Lett. 30 (24), 8044.